# CASSCF/CI calculations of electronic states and potential energy surfaces of PtH2

K. Balasubramanian

Citation: The Journal of Chemical Physics **87**, 2800 (1987); doi: 10.1063/1.453068
View online: http://dx.doi.org/10.1063/1.453068
View Table of Contents: http://scitation.aip.org/content/aip/journal/jcp/87/5?ver=pdfcov
Published by the AIP Publishing

# CASSCF/CI calculations of electronic states and potential energy surfaces of $PtH_2$

K. Balasubramanian[a)]
*Department of Chemistry, Arizona State University, Tempe, Arizona 85287*

(Received 31 March 1987; accepted 11 May 1987)

Complete active space MCSCF followed by MRSDCI (multireference singles and doubles configuration interaction) calculations are carried out on the electronic states of $PtH_2$. Spin–orbit interaction is introduced using a relativistic configuration interaction scheme on $PtH^+$ whose $d$ orbital Mulliken population is close to that of the $d$ population of $PtH_2$ and thus enables calculation of spin–orbit splittings for the electronic states of $PtH_2$. The bending potential energy surfaces of the $^1A_1$ and $^3A_1$ states are obtained. The $^1A_1$ surface has a bent minimum and dissociates almost without a barrier into $Pt(^1S_0)$ and $H_2$, while the $^3A_1$ state has a large ($\sim$55 kcal/mol) barrier to dissociation into $Pt(^3D_3) + H_2$. The ground state of $PtH_2$ is a bent $^1A_1$ state ($\theta = 85°$).

## I. INTRODUCTION

Electronic structure and reactivities of transition metal clusters is a topic of a number of investigations in recent years.[1–7] An important question relates to the reactivity trends of these clusters as a function of cluster size. The $MH_2$ molecules (where M = transition element) serve as a useful small model for studying the reactivities of these species. Platinum is one of the most important materials for heterogeneous catalysis of hydrogenation since the hydrogenation energy is much smaller for this system than other comparable systems such as Pd and Ni.[8,9] The reactivities of even Pt atoms with the $H_2$ molecule have not been studied using CASSCF/CI techniques both due to large number of electrons, correlation, and relativistic effects. The only previous *ab initio* investigation on $PtH_2$ is the GVB/small CI study of Low and Goddard[32] on reductive coupling of H–H bond with Pd and Pt.

Relativistic effects such as mass–velocity, Darwin, and spin–orbit interaction are very important for molecules containing very heavy atoms.[10–13] Wang and Pitzer[14] have shown the importance of these effects for PtH and $PtH^+$. These authors have shown that spin–orbit contamination of open-shell $\lambda$–$s$ states of the PtH diatomic are nonnegligible. Motivated by both theoretical and experimental interest on platinum-containing systems and to understand the reactivity of the platinum atom with $H_2$ we undertake the present investigation. Further, the electronic structure properties of molecules containing heavy atoms is a topic of significant activity in recent years.[10–19]

## II. METHOD OF INVESTIGATION

The $PtH_2$ molecule was oriented in the $yz$ plane as shown in Fig. 1. The linear structure was oriented along the $y$ axis. We employ relativistic effective core potentials including spin–orbit interaction for the platinum atom. The use of effective core potentials in molecular structure calculations was reviewed by Krauss and Stevens[19] and more recently by Christiansen *et al.*[13] and Balasubramanian and Pitzer.[12] Gaussian fits of relativistic effective core potentials have been generated by Ermler and Christiansen[20] recently. Wang and Pitzer[14] have employed analogous numerical potentials which have been shown to give reliable results for the PtH diatomic. Ermler and Christiansen[20] have also optimized a $(3s3p3d)$ valence Gaussian basis set for the Pt atom. We employ this basis set together with the potentials generated by these authors retaining the $5d^9 6s^1$ outer shell in the valence space. Although inclusion of the $5s$ and $5p$ semicore orbitals might improve the results, calculations of Wang and Pitzer[14] indicate that the $5d^9 6s^1$ potentials offer very good results. We contract the two large exponent $p$ functions to generate a $(3s2p3d)$ basis set. This basis is shown in Table I. For the hydrogen atoms we employ van Duijneveld's[21] $(5s|3s)$ basis set augmented by a set of $p$-type polarization functions with the exponent of 0.9. The hydrogen basis exponents were multiplied by a scaling factor of 1.44. This hydrogen basis was employed by Balasubramanian and McLean[22] in their $SiH_2$ calculations.

First MCSCF calculations were carried out on $PtH_2$ to generate the orbital space for configuration interaction calculations. The MCSCF calculations carried out were complete active space MCSCF (CASSCF) calculations. For $PtH_2$, there are 12 active (valence) electrons. In the CASSCF method the active electrons are distributed in all possible ways among a chosen set of most important orbitals referred to as the internal space of orbitals. For the orienta-

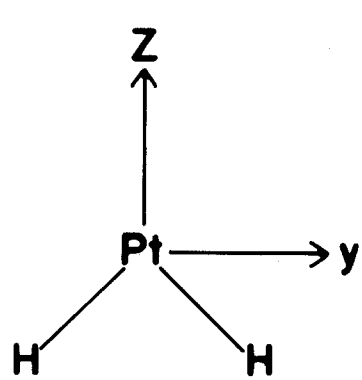


FIG. 1. Orientation of the $PtH_2$ molecule.

[a)] Alfred P. Sloan Fellow; Camille and Henry Dreyfus Teacher–Scholar.

 0021-9606/87/172800-06$02.10 

TABLE I. Valence Gaussian basis set for the Pt atom.

| | Exponent | Contraction coefficient |
|---|---|---|
| $s$ | 0.4324 | 1.0 |
| $s$ | 0.236 | 1.0 |
| $s$ | 0.0606 | 1.0 |
| $p$ | 0.7393 | 0.03 |
| $p$ | 0.1231 | 0.30 |
| $p$ | 0.0412 | 1.0 |
| $d$ | 1.2692 | 1.0 |
| $d$ | 0.4691 | 1.0 |
| $d$ | 0.1539 | 1.0 |

tion of the molecule shown in Fig. 1, the outer $d$ and $s$ orbitals of Pt and $s$ orbitals of hydrogen atoms span $5a_1$ ($d_{x^2}$,$d_{y^2}$,$d_{z^2}$,$s$); H($s_1 + s_2$), $2b_2$, $1b_1$, and $1a_2$ orbitals at infinite separation. Note that the real $d_{x^2}$, $d_{y^2}$, and $d_{z^2}$ are all treated in an equivalent way since this is required by the ALCHEMY II sets of codes which use the square density method to generate MCSCF orbitals. This leads to a CASSCF in which an extra $a_1$ orbital is retained. Thus, our CASSCF calculations included $5a_1$, $2b_2$, $1b_1$, and $1a_2$ orbitals in the active space.

Configuration interaction calculations are carried out following CASSCF. The CI calculations carried out were MRSDCI (multireference singles and doubles) calculations. The MRSDCI calculations included all configurations in the CASSCF with coefficients $\geqslant 0.07$ for a given state as reference configurations. Single and double excitations are allowed from these reference configurations. The dimensions of the CASSCF and CI spaces are shown in Table II.

The effect of spin–orbit interaction on the electronic states of $PtH_2$ was estimated using relativistic configuration interaction (RCI) calculations on $PtH^+$. The $PtH^+$ system was chosen for two reasons: (i) the spin multiplicities of the electronic states of $PtH^+$ match with those of $PtH_2$; (ii) the Mulliken population analysis of the electronic states of $PtH^+$ and $PtH_2$ show that the $d$ orbital population of the corresponding states is very close. Since the spin–orbit coupling of these systems are determined by the $d$ population of the Pt atom (since the spin–orbit contribution due to $s$ orbitals on Pt and H are zero), comparison of the $PtH^+$ spin–orbit splitting is meaningful. Our past calculations in the following pairs (PbF,[23] PbH[24]) (BiH,[25] BiF[26]) seem to suggest that the spin–orbit splittings of these systems are related to the electronic state of the heavy atom in the molecule.

RCI calculations on $PtH^+$ included all $\lambda$–$s$ configurations which give rise to a $\omega$–$\omega$ state of given symmetry as reference configurations. Single and double excitations were included from these reference configurations. A similar RCI calculation was also carried out on the $^3D_3$, $^3D_1$, $^1S_0$ states of the Pt atom. The CASSCF and MRSDCI calculations in the absence of spin–orbit interaction were carried out using the present authors[27] modification of ALCHEMY II codes[28] to include relativistic effective core potentials. The RCI calculations were carried out using the present author's modified version of the code to carry out relativistic CI based on the method in Ref. 29.

TABLE II. Dimensions of the CASSCF and MRSDCI spaces. Configuration counts are in $C_{2v}$ symmetry.

| State | CASSCF | MRSDCI | |
|---|---|---|---|
| | | Linear | Bent |
| $^1A_1$ | 690 | 20 047 | 39 199 |
| $^3A_1$ | 831 | 35 270 | ··· |
| $^3B_1$ | 861 | 37 007 | ··· |
| $^1B_1$ | 602 | 59 684 | ··· |
| $^3A_2$ | 861 | 54 993 | ··· |
| $^1A_2$ | 602 | 33 344 | ··· |

## III. RESULTS AND DISCUSSION

### A. Pt atom

Calculations on some of the Pt atomic states (described below) were made to test the reliability of the effective core potentials as well as to study the effect of spin–orbit interaction. Since our RCI code is interfaced with a code that uses Slater-type orbitals we employed a double-zeta STO basis used by Wang and Pitzer[14] in their PtH calculations. Atomic orbitals were generated for the $^3D(d^9s^1)$ electronic state without spin–orbit interaction. RCI calculations were carried out on the $^3D_3(d^9_{5/2}s\alpha)$, $^3D_1(d^9_{3/2}s\beta)$, and $^1S_0(d^{10})$ states. The RCI calculations included single and double excitations from reference configurations which give rise to $^3D_3$, $^3D_1$, and $^1S_0$ states. Another CI calculation was also carried out this time suppressing the spin–orbit interaction. Results of these calculations and the corresponding experimental values are reported in Table III. As one can see the experimental splitting of the $^3D_3$–$^3D_1$ states and $^3D_3$–$^1S_0$ states are in very good agreement with our calculated results. It is also pointed out that the $^3D_3$–$^3D$ (no spin–orbit) splitting is 0.019 94 hartrees a.u. This value is useful in correcting energies obtained without spin–orbit interaction in the near dissociation limits. The $^1S_0$–$^1S$ splitting is however, relatively small (0.003 56 hartrees). Thus, the error introduced in calculating the closed shell $^1A_1$ state of $PtH_2$ which dissociates into $Pt(^1S_0) + H_2$ would be smaller. Note that the $^3D_3$–$^3D_1$ splitting corresponds to the splitting of the $d^9_{5/2}$–$d^9_{3/2}$ spinor of the Pt atom and is quite large.

### B. $PtH^+$

Relativistic CI calculations on the electronic states of $PtH^+$ were carried out with the objective of estimating

TABLE III. Spin–orbit splittings for Pt.

| State | Theory | Experiment[a] |
|---|---|---|
| $^3D_3(d^9_{5/2}s\alpha)$ | 0.0 | 0.0 |
| $^3D_1(d^9_{3/2}s\beta)$ | 10 076 | 10 132 |
| $^1S_0(d^{10})$ | 5 705 | 6 140 |
| $^3D$ | 4 376 | ··· |
| $^1S$ | 6 486 | ··· |

[a] Reference 31.

spin–orbit effects on $PtH_2$. In general all $\lambda$–$s$ configurations which give rise to $\omega$–$\omega$ states of the same symmetry were mixed in the RCI calculations. The $0^+$ state included five Cartesian reference configurations arising from $^1\Sigma_{0^+}^+$ and $^3\Pi_{0^+}$. The $0^-$ state included four Cartesian reference configurations arising from the $^3\Pi_{0^-}$ state. The 3-state calculations included two reference configurations arising from $^3\Delta_3$. The 2-state included reference configurations from $^3\Delta_2$, $^1\Delta_2$, and $^3\Pi_2$ (six reference configurations) while the 1 state included $^3\Delta_1$, $^3\Pi_1$, and $^1\Pi_1$ reference configurations. Single and double excitations were allowed from these reference configurations. CI calculations were also carried out in the absence of spin–orbit interaction. The energies of all the electronic states of $PtH^+$ are reported at 3.10 bohr in Table IV. This distance was chosen since this corresponds to the equilibrium geometry of the PtH ground state. In that table, we also show the actual contributions of various $\lambda$–$s$ states. As one can see from that table the spin–orbit contamination and spin–orbit effects are nonnegligible for systems containing the Pt atom. CASSCF/FOCI calculations were also carried out on $PtH^+$ at 3.10 bohr with the objective of calculating the Mulliken population analysis of the electronic states of $PtH^+$ to compare these values with analogous $PtH_2$ states. These Mulliken populations are discussed in the section on $PtH_2$.

### C. $PtH_2$

Table V shows the CASSCF and MRSDCI geometries and energies of electronic states of $PtH_2$ in the absence of spin–orbit interaction. As one can see from that table the ground state of $PtH_2$ is the bent $^1A_1$ state. The bending angle at MRSDCI level is 85.1°. The Pt–H bond length is 1.52 Å. It must be noted that this bond length is almost identical to the experimental bond length of the PtH $^2\Delta_{5/2}$ state which is 1.53 Å.[30]

For the linear geometry the $^3\Delta_g$ state is the lowest electronic state in the absence of spin–orbit interaction. The $^3\Pi_g$ state is above $^3\Delta_g$. The $^3\Delta_g$–$^3\Pi_g$ splitting of the linear $PtH_2$ is 4267 $cm^{-1}$ in the absence of spin–orbit coupling. The Pt–H bond lengths of the linear states are about 0.15–0.22 Å larger than the Pt–H bond length of the bent $^1A_1$ ground state.

Bond lengths shrink up to 0.03 Å for $PtH_2$ due to correlation effects included in MRSDCI calculations in comparison to the CASSCF calculations. This shrinking is relatively small and thus CASSCF calculations give reliable bond lengths. The bending angle for the $^1A_1$ state changes by about 2°. The energies of different electronic states are influenced to a considerable extent by correlation effects. For example the $^1A_1$ (bent)–$^3\Delta_g$ CASSCF splitting is 2.01 eV in comparison to an MRSDCI splitting of 2.47 eV. This suggests that correlation effects are significant for the $^1A_1$ bent ground state.

Table VI reports separation of electronic states of $PtH_2$ corrected for spin–orbit interactions. The spin–orbit splittings are estimated from the corresponding electronic states of the diatomic $PtH^+$ reported in Table IV. For example, the $^3\Delta_3$–$^3\Delta$ splitting is 4359 $cm^{-1}$ (Table VI). This correction is then introduced to the MRSDCI energies of the $PtH_2$ molecular states. (For example, the $^3\Delta_3$ state is lowered by 4300 $cm^{-1}$ relative to the $^3\Delta_g$ state obtained from MRSDCI calculations.) We believe that the spin–orbit splitting estimated this way are accurate to $\pm$ 0.2 eV. We use the $PtH^+$ system for comparison since the Mulliken $d$ population of the Pt atom which determines the spin–orbit splitting in $PtH^+$ and $PtH_2$ are very similar as we discuss later. The $^3\Delta_3$–$^3\Delta$, $^3\Pi_{0^-}$–$^3\Pi$, $^3\Pi_{0^+}$–$^3\Pi$, $^1\Sigma_{0^+}^+$–$^1\Sigma$ splittings should be quite accurate. The $^3\Delta_1$–$^3\Delta$, $^3\Pi_1$–$^3\Pi$, $^3\Delta_2$–$^3\Delta$, $^3\Pi_2$–$^3\Pi$, $^1\Pi_1$–$^1\Pi$ splittings, however, could be influenced by spin–orbit contaminations. However, such contaminations lower one state while increasing the energy of the upper state. This effect has been taken into account in the $PtH^+$ calculations. The only difference could be in the amount of spin–orbit contamination. The error bar we have introduced is mainly for this.

The bending potential energy curves of two important states of $PtH_2$ [$^1A_1$,$^3A_1$($^3\Delta_g$)] are shown in Fig. 2. The curves were obtained with the CASSCF method. The reason for choosing two different spin multiplets is to differentiate the reactivities of the singlet and triplet states. The bond lengths were optimized for every angle. The dotted curves are the estimated surfaces which included spin–orbit interaction. The 5411-CASSCF leads to a small size consistency error in the dissociation limit. At this level the $d^8s^2$ (triplet) is lower than $d^9s^1$ (triplet), although CI calculations correct this. To estimate the correct dissociation limits and the effect of spin–orbit interaction we calculated the $^3D_3$–$^3D$ splitting and corrected this for the curve without spin–orbit interaction. A similar correction was carried out for the linear state by comparing with the spin–orbit splitting of $PtH^+$. It should be noted that the $^3D_3$–$^3D$ splitting of the atom and $^3\Delta_g$–$3_g$ splitting are within 17 $cm^{-1}$ assuring that the procedure could not be off too much. A similar behavior was observed for the singlet state. The effects of spin–orbit interaction for other bending angles were obtained using a simple lever rule. The curves were shifted parallel to the curves in the absence of spin–orbit coupling. This would be true only for the $^3g$ component of $^3\Delta$ and $0_g^+$ component of $^1\Sigma_g^+$ since

TABLE IV. Electronic state of PtH.[a]

| State | Energy | Assignment |
|---|---|---|
| $^1\Sigma_{0^+}^+$ | 0.0 | 77% $^1\Sigma^+$, 6% $^3\Pi_{0^+}$ |
| $^1\Sigma^+$ | 1 655 | |
| $^3\Delta_3$ | 4 265 | $^3\Delta_3$ |
| $(^3\Delta + ^3\Pi)_2$ | 6 229 | 80% $^3\Delta_2$, 11% $^3\Pi_2$, 3% $^1\Delta_2$ |
| $(^3\Delta + ^3\Pi + ^1\Pi)_1$ | 8 515 | 52% $^3\Delta_1$, 25% $^3\Pi_1$, 16% $^1\Pi_1$ |
| $^3\Delta$ | 8 624 | |
| $(^3\Pi + ^1\Delta + ^3\Delta)_2$ | 12 401 | 76% $^3\Pi_2$, 13% $^1\Delta_2$, 6% $^3\Delta_2$ |
| $^3\Pi$ | 14 742 | |
| $(^3\Pi + ^3\Delta)_1$ | 16 218 | 67% $^3\Pi_1$, 27% $^3\Delta_1$ |
| $^1\Pi$ | 16 412 | |
| $^3\Pi_0$ | 16 624 | $^3\Pi_0$ |
| $^3\Pi_{0^-}$ | 17 592 | 87% $^3\Pi_{0^-}$, 6% $^1\Sigma_{0^+}^+$ |
| $(^1\Pi + ^3\Delta)_1$ | 17 944 | 74% $^1\Pi_1$, 15% $^3\Delta_1$, 2% $^3\Pi_1$ |

[a] All separations were calculated at 3.1 bohr.

TABLE V. Geometries and energies of electronic states of $PtH_2$.

| | CASSCF | | | MRSDCI | | |
|---|---|---|---|---|---|---|
| | $r$ (Å) | $\theta$ (deg) | $E^a$ | $r$ (Å) | $\theta$ (deg) | $E^a$ |
| $^1A_1$ | 1.55 | 87 | − 27.376 209 9 | 1.52 | 85.1 | − 27.529 442 |
| $^1\Sigma_g^+$ | 1.70 | 180.0 | 1.90 | 1.675 | 180.0 | 2.33 |
| $^3\Delta_g$ | 1.70 | 180.0 | 2.01 | 1.69 | 180.0 | 2.47 |
| $^3A_1$[b] | 1.80 | 110.0 | 4.33 | ... | ... | ... |
| $^3\Pi_g$ | 1.73 | 180 | 2.59 | 1.71 | 180.0 | 2.995 |
| $^1\Pi_g$ | 1.74 | 180 | 2.63 | 1.71 | 180.0 | 3.02 |
| $^1\Delta_g$ | 1.72 | 180 | 4.18 | 1.69 | 180.0 | 4.98 |

[a] Energy of the bent $^1A_1$ state is in hartrees. All other energies are in eV with respect to the $^1A_1$ bent state.
[b] Saddle point (estimated).

these are the largest $\Omega$ components of the corresponding $\lambda$–$s$ states. For other states such as $^3\Delta_1$, etc., avoided crossings could change the shapes of the curves.

As one can see in Fig. 2, the $^3\Delta_g$ curve has a relatively large barrier dissociation into $Pt(^3D) + H_2$ while the singlet curve has a bent minimum but dissociates into $Pt(^1S) + H_2$ almost without a barrier. The spontaneous insertion of $Pt(^1S_0)$ into $H_2$ to form $PtH_2(^1A_1)$ was also predicted earlier by Low and Goddard[32] using the GVB method. This would imply that the $^1S_0$ state of the Pt atom would insert into $H_2$ almost spontaneously to form a bound $PtH_2$ molecule while the $^3D_3$ state would not react with $H_2$ as a result of the barrier. The barrier height and saddle-point geometry could not be calculated exactly due to the difficulties in locating the saddle point. Furthermore, there is a rapid change in the bond length near the saddle point of $^3A_1$ surface. The linear MCSCF bond length of 1.70 Å gradually increases as the bond angle increases until one reaches the near vicinity of the saddle point. For $\theta = 110°$, if one starts with large angle guess, the Pt–H bond length obtained is 1.795 Å. The bond length rapidly falls to 1.60 Å for $\theta = 100°$ and continues to fall to 1.59 Å for $\theta = 70°$ and then rises gradually to large bond lengths for smaller angles so that the molecule would dissociate into $Pt + H_2$. As mentioned above, the bond length of the saddle point can only be estimated since there is a sharp change in the potential energy surface as one can see in Fig. 2. We report in Table V the bond length for $\theta = 110°$ obtained using the linear-like input guess. The saddle point ($\theta = 110°$) was estimated by joining the curves obtained for angles below and above these values smoothly. Thus, the geometry reported in Table V is only an estimate and changes sharply if $\theta$ shifts to 100°. Thus, the calculated barrier height of 56 kcal/mol with respect to the linear geometry is only a crude estimate. The effect of spin–orbit interaction on the barrier height $3_g$ (linear) component of the $^3\Delta_g$ surface is, however, estimated to be small (~2 kcal/mol) since both the saddle point and linear structure lower to the same extent for this component.

The importance of electron correlation can be seen by an inspection of the leading configurations of the CASSCF-CI wave function of the electronic states of $PtH_2$. Table VII

TABLE VI. Estimated separations of electronic states of $PtH_2$ including spin–orbit contributions.

| State | $E$ (eV)[a] |
|---|---|
| $^1A_1$(bent) | − 0.18 |
| $^3g(^3\Delta_g)$ | 1.94 |
| $0_g^+(^1\Sigma_g^+)$ | 2.12 |
| $2_g(^3\Delta_g + ^3\Pi_g)$ | 2.18 |
| $^1\Sigma_g^+$ | 2.33 |
| $1_g(^3\Delta_g + ^3\Pi_g + ^1\Pi_g)$ | 2.46 |
| $^3\Delta_g$ | 2.47 |
| $2_g(^3\Pi_g + ^1\Delta_g + ^3\Delta_g)$ | 2.70 |
| $^3\Pi_g$ | 2.99 |
| $^1\Pi_g$ | 3.02 |
| $1_g(^3\Pi_g + ^3\Delta_g + ^1\Pi_g)$ | 3.17 |
| $1_g(^1\Pi_g + ^3\Pi_g + ^3\Delta_g)$ | 3.21 |
| $0_g^-(^3\Pi_g)$ | 3.22 |
| $0_g^+(^3\Pi_g)$ | 3.34 |

[a] Separations with respect to the bent $^1A_1$ state in the absence of spin–orbit interaction ( − 27.529 44 hartree a.u.).

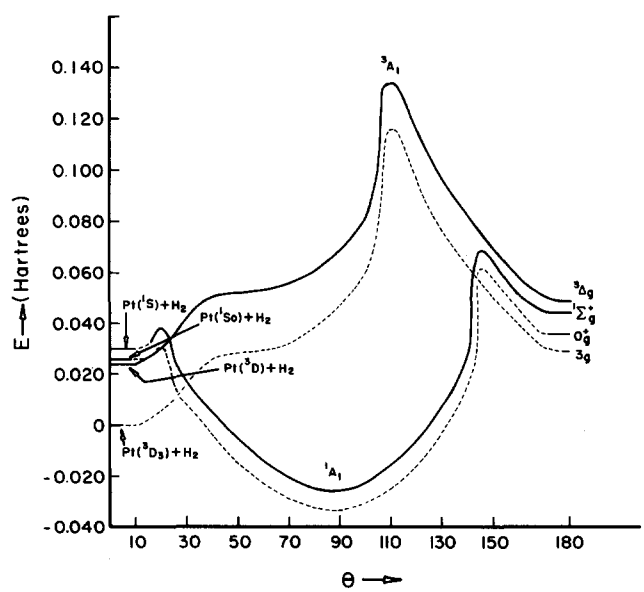


FIG. 2. CASSCF bending potential energy surfaces for the $^1A_1$ and $^3A_1$ states of $PtH_2$. The dotted curves are estimated surfaces including spin–orbit interaction.

TABLE VII. CASSCF-CI wave functions of electronic states of $PtH_2$.

| Coefficient | $1a_1$ | $2a_1$ | $3a_1$ | $4a_1$ | $1b_2$ | $2b_2$ | $1b_1$ | $1a_2$ |
|---|---|---|---|---|---|---|---|---|
| | | | | $^1A_1$ (bent) | | | | |
| 0.969 | 2 | 2 | 2 | 0 | 2 | 0 | 2 | 2 |
| −0.119 | 2 | 2 | 2 | 0 | 2 | 2 | 2 | 2 |
| 0.116 | 1 | 2 | 2 | 1 | 1 | 1 | 2 | 2 |

| Coefficient | $1\sigma_g$ | $2\sigma_g$ | $3\sigma_g$ | $1\sigma_u$ | $1\delta_g$ | $1\pi_g$ |
|---|---|---|---|---|---|---|
| | | | | $^3\Delta_g$ | | |
| −0.99 | 2 | 1 | 0 | 2 | 3 | 4 |
| 0.085 | 2 | 1 | 2 | 0 | 3 | 4 |
| | | | | $^3\Pi_g$ | | |
| 0.948 | 2 | 1 | 0 | 2 | 4 | 3 |
| 0.276 | 2 | 2 | 0 | 2 | 3 | 3 |
| −0.083 | 2 | 2 | 1 | 0 | 4 | 3 |
| | | | | $^1\Delta_g$ | | |
| 0.855 | 2 | 1 | 0 | 2 | 3 | 4 |
| −0.483 | 2 | 2 | 0 | 2 | 4 | 2 |
| −0.083 | 2 | 2 | 1 | 0 | 3 | 4 |
| | | | | $^1\Sigma_g^+$ | | |
| −0.882 | 2 | 0 | 0 | 2 | 4 | 4 |
| 0.317 | | | | | | |
| 0.317[a] | 2 | 2 | 0 | 2 | 2 | 4 |
| | | | | $^1\Pi_g$ | | |
| 0.905 | 2 | 1 | 0 | 2 | 4 | 3 |
| 0.389 | 2 | 2 | 0 | 2 | 3 | 3 |
| −0.091 | 2 | 1 | 2 | 0 | 4 | 3 |

[a] The coefficients are for $\delta^2_{x^2-z^2}$ and $\delta^2_{xz}$.

shows the coefficients of the important configurations contributing to the electronic states of $PtH_2$.

Table VIII shows the Mulliken population analysis of the natural orbitals of $PtH_2$ and $PtH^+$ for various electronic states obtained from MRSDCI calculations. First we note that the total gross populations of the Pt atom for all the linear $PtH_2$ electronic states are about the same (9.5). However, the bent $^1A_1$ ground state exhibits an enhanced $d$ population accompanied by a reduction of the hydrogen $s$ population. The $p$ population is considerably larger for the linear states than the bent $^1A_1$ state. The gross $d$ populations of the $^3\Delta_g$, $^3\Pi_g$, $^1\Delta_g$, etc., are between 8.5–8.6 but the $^1\Sigma_g^+$ state has a slightly enhanced 8.8 $d$ population as anticipated. The $PtH^+$ electronic states exhibit the same trend. The gross $d$ population of the $^3\Delta_g$, $^3\Pi_g$, etc. are between 8.64–8.67 while the $^1\Sigma_g^+$ state has a gross $d$ population of 8.9. The similarity between the $d$ populations of $PtH^+$ and $PtH_2$ can be rationalized as follows. The $1\sigma_u$ orbital of the linear structure is mainly H($s$) with some Pt($p$) which is mainly from the $\sigma_u$ orbital, the hydrogen population of the $1\sigma_u$ orbital is found to be 1.63. Since the overall H population is about 2.45, the $\sigma_g$ bonding hydrogen population is found to be 0.82 which is close to the hydrogen population of 0.87 in $PtH^+$. Thus, the bonding of Pt and H in the $\sigma_g$ ($\sigma$) space is about the same in $PtH^+$ and linear $PtH_2$. The $\delta_g$, $\pi_g$ orbitals are nonbonding in both $PtH^+$ and $PtH_2$ as expected. This is the basis for using the $PtH^+$ system to estimate the spin–orbit effects of the electronic states of $PtH_2$.

## IV. CONCLUSION

Electronic states of $PtH_2$ as well as the Pt atom and $PtH^+$ were investigated using a CASSCF/CI scheme. Spin–orbit effects are estimated through RCI (relativistic CI) calculations on $PtH^+$. The bending potential energy surfaces of the $^1A_1$ and $^3A_1$ states of $PtH_2$ were investigated. The $^3A_1$ surface has a barrier while the $^1A_1$ state has a bent minimum. The reactivities of the Pt($^1S_0$) and Pt($^3D_3$) states are contrasted. It is predicted that the Pt($^1S_0$) state would insert into $H_2$ almost spontaneously to form the bent $PtH_2$ ground state while the $^3D_3$ state would not react with $H_2$ spontaneously.

## ACKNOWLEDGMENT

This research was supported by the U.S. Department of Energy under Grant No. DEFG02-86-ER13558.

TABLE VIII. Mulliken population analysis for $PtH_2$ and Pt–$H^+$.

| | Net | | | | | | Gross | | | | | | |
|---|---|---|---|---|---|---|---|---|---|---|---|---|---|
| State | Pt | H | Pt($d$) | Pt($s$) | Pt($p$) | H($s$) | Pt | H | Pt($d$) | Pt($s$) | Pt($p$) | H($s$) | Overlap |
| $^3\Delta_g$ | 8.969 | 1.918 | 8.227 | 0.314 | 0.147 | 1.908 | 9.525 | 2.475 | 8.556 | 0.599 | 0.371 | 2.447 | 1.114 |
| $^1\Sigma_g^+$ | 8.95 | 1.929 | 8.490 | 0.155 | 0.141 | 1.918 | 9.513 | 2.487 | 8.787 | 0.361 | 0.365 | 2.459 | 1.117 |
| $^1\Delta_g$ | 8.968 | 1.893 | 8.268 | 0.328 | 0.099 | 1.890 | 9.538 | 2.462 | 8.600 | 0.610 | 0.327 | 2.443 | 1.138 |
| $^3\Pi_g$ | 8.939 | 1.953 | 8.148 | 0.368 | 0.139 | 1.942 | 9.493 | 2.507 | 8.473 | 0.666 | 0.354 | 2.478 | 1.108 |
| $^1\Pi_g$ | 9.967 | 1.944 | 8.155 | 0.376 | 0.136 | 1.933 | 9.512 | 2.488 | 8.489 | 0.674 | 0.348 | 2.459 | 1.089 |
| $^1A_1$[a] | 9.42 | 1.49 | 8.72 | 0.47 | 0.12 | 1.48 | 9.96 | 2.04 | 9.13 | 0.75 | 0.086 | 1.991 | 1.092 |
| $PtH^+$ | | | | | | | | | | | | | |
| $^3\Delta_g$ | 8.83 | 0.598 | 8.358 | 0.185 | 0.009 | 0.598 | 9.116 | 0.884 | 8.67 | 0.41 | 0.032 | 0.884 | 0.572 |
| $^1\Sigma_g^+$ | 8.86 | 0.61 | 8.667 | 0.057 | 0.007 | 0.607 | 9.128 | 0.872 | 8.92 | 0.181 | 0.027 | 0.872 | 0.529 |
| $^3\Pi_g$ | 8.81 | 0.63 | 8.357 | 0.189 | .009 | 0.63 | 9.088 | 0.912 | 8.639 | 0.415 | 0.034 | 0.91 | 0.563 |

[a] Bent geometry.

[1]M. E. Geusic, M. D. Morese, and R. E. Smalley, J. Chem. Phys. **82**, 590 (1985).
[2]M. D. Morse, M. E. Geusic, J. R. Health, and R. E. Smalley, J. Chem. Phys. **82**, 2293 (1985).
[3]R. C. Batezold and J. F. Hamilton, Progr. Solid State Chem. **15**, 1 (1983).
[4]D. E. Powers, S. G. Hansen, M. E. Geusic, D. L. Michalopoulos, and R. E. Smalley, J. Chem. Phys. **78**, 2866 (1983).
[5]M. D. Morse, Chem. Rev. **86**, 1049 (1986).
[6]*Theory of Chemisorption*, edited by J. M. Smith (Springer, Berlin, 1980).
[7]P. R. R. Langridge-Smith, M. D. Morse, S. G. Hansen, R. E. Smalley, and A. J. Mera, J. Chem. Phys. **80**, 5400 (1980).
[8]K. Christman, G. Ertl, and T. Pignet, Surf. Sci. **54**, 365 (1976).
[9]J. E. Demuth, Surf. Sci. **65**, 369 (1977).
[10]K. S. Pitzer, Acc. Chem. Res. **12**, 271 (1979).
[11]K. S. Pitzer, Int. J. Quantum Chem. **25**, 131 (1984).
[12]K. Balasubramanian and K. S. Pitzer, Adv. Chem. Phys. **67**, 287 (1987).
[13]P. A. Christiansen, W. C. Ermler, and K. S. Pitzer, Annu. Rev. Phys. Chem. **36**, 407 (1985).
[14]S. W. Wang and K. S. Pitzer, J. Chem. Phys. **79**, 3851 (1983).
[15]K. Balasubramanian, Chem. Phys. Lett. **135**, 288 (1987).
[16]K. Balasubramanian, J. Chem. Phys. **85**, 1443 (1986).
[17]K. Balasubramanian, J. Chem. Phys. **85**, 3401 (1986).
[18]K. Balasubramanian, J. Mol. Spectrosc. **115**, 258 (1986).
[19]M. Krauss and W. J. Stevens, Annu. Rev. Phys. Chem. **35**, 357 (1984).
[20]W. C. Ermler and P. A. Christiansen (private communications).
[21]F. B. van Duijneveldt, IBM Rep. 945 (1971).
[22]K. Balasubramanian and A. D. McLean, J. Chem. Phys. **85**, 5117 (1986).
[23]K. Balasubramanian, J. Chem. Phys. **83**, 2311 (1985).
[24]K. Balasubramanian and K. S. Pitzer, J. Phys. Chem. **88**, 1146 (1984).
[25]K. Balasubramanian, Chem. Phys. Lett. **114**, 201 (1985).
[26]K. Balasubramanian, Chem. Phys. Lett. **127**, 324 (1986).
[27]K. Balasubramanian, Chem. Phys. Lett. **127**, 585 (1986).
[28]The major authors of ALCHEMY II codes are B. Liu, B. Lengsfield, and M. Yoshimine.
[29]P. A. Christiansen, K. Balasubramanian, and K. S. Pitzer, J. Chem. Phys. **76**, 5087 (1982).
[30]K. P. Huber and G. Herzberg, *Spectroscopic Constants of Diatomic Molecules* (Van Nostrand, Princeton, 1979).
[31]C. E. Moore, *Table of Atomic Energy Levels*, Natl. Bur. Stand. (U.S. GPO, Washington, D.C., 1971).
[32]J. J. Low and W. A. Goddard III, Organometal. **5**, 609 (1986).